Received: 27 October 2023 | Revised: 13 March 2024 | Accepted: 22 March 2024

DOI: 10.1111/jace.19834

Journal of the American Ceramic Society

RESEARCH ARTICLE

Effect of texture on ultra-high strain behavior in eco-friendly NBT-0.25ST ceramics using NBT template

Ayse Berksoy-Yavuz[1] | **Mustafa Yunus Kaya**[2] | **Ezgi Yalcin**[3] | **Namik Kemal Gozuacik**[3] | **Ebru Mensur**[3]

[1]Department of Metallurgical and Materials Engineering, Faculty of Engineering, Istanbul Gedik University, Istanbul, Turkey

[2]Department of Metallurgical and Materials Engineering, Faculty of Engineering and Natural Sciences, Bursa Technical University, Bursa, Turkey

[3]Department of Materials Science and Engineering, Gebze Technical University, Kocaeli, Turkey

Correspondence
Ayse Berksoy-Yavuz, Department of Metallurgical and Materials Engineering, Faculty of Engineering, Istanbul Gedik University, 34876 Kartal, Istanbul, Türkiye.
Email: ayse.yavuz@gedik.edu.tr

Funding information
Bursa Technical University, Scientific Research Projects Coordinatorship, Grant/Award Number: 211N046; TUBITAK ULAKBIM

Abstract

<001> oriented textured $(Na_{0.5}Bi_{0.5}Ti)O_3$-0.25$SrTiO_3$ (NBT-0.25ST) system was fabricated using 10 mol% plate-like NBT template particles to enhance the electrical properties. Random and textured samples were prepared by a tape-casting method. Lotgering factor for textured sample was calculated as 88%. Dielectric values of the samples were comparable, and this means texturing using NBT samples of this orientation did not change the dielectric constant. The maximum unipolar strain values of random and textured NBT-0.25ST systems were found to be as ~0.09% and ~0.59%, respectively. This current study emphasizes the significant difference in maximum unipolar strain values between the random and textured versions of the NBT-0.25ST system, indicating the superiority of the textured material in terms of responsiveness to the electric field. The FOM under high electric fields of textured and random NBT-0.25ST was found to increase almost 45-fold compared with random case.

KEYWORDS
lead-free, orientation, texture, ultra-high strain

1 | INTRODUCTION

Over the decades, lead-based piezoelectric ceramics have played a crucial role in many vast applications for instance actuators, transducers, capacitors, ultrasonic motors, and sonars in the global electronic device industry.[1–5] Lead-based binary or ternary piezoceramic systems such as $Pb(Zr,Ti)O_3$ (PZT), $Pb(Mg_{1/3}Nb_{2/3})O_3$–$PbTiO_3$ (PMN-PT), $Pb(Zn_{1/3}Nb_{2/3})O_3$-$Pb(Zr_yTi_{1-y})O_3$ (PZN-PZT), and $Pb(In_{1/2}Nb_{1/2})$-$Pb(Mg_{1/3}Nb_{2/3})O_3$–$PbTiO_3$ (PIN-PMN-PT) have been widely investigated for a long time due to their superior electrical and electromechanical properties.[1,6–9] However, lead-based ceramics threaten human and environmental health, and increasing environmental concerns have become crucial in the development of comparable lead-free piezoelectric materials since 2003, as their use has been restricted by regulations.[10,11] Among the most promising environmentally friendly alternative lead-free materials, $(Na_{0.5}Bi_{0.5})TiO_3$ (NBT) based perovskites exhibit high remnant polarization (P_r~38 kV/cm), low dielectric loss (tan δ), and high Curie temperature (T_C~320°C). Meanwhile, a high coercive field (E_c~63 kV/cm) of unmodified NBT hinders the poling process at a low electric field and the large leakage current is

also a disadvantage in poling.[12,13] Besides these disadvantages, NBT ceramics can exhibit interesting piezoelectric properties such as ultra-high strain, electrostrictive effect, or enhanced energy storage performance based on different phase transitions mechanisms in solid solution compositions enabled by the addition of $BaTiO_3$ (BT), $SrTiO_3$ (ST), or $NaNbO_3$ (NN) compounds.[13–16] Ultra-high strain can be associated with a reversible phase transition from the nonpolar relaxor state (ergodic relaxor) to the polar state with the long-range ferroelectric arrangement by an induced-electric field that was verified with the studies on NBT-based systems.[17,18] Induced ultra-high strain via electric field application is a critical parameter in driving advanced technological systems such as ultrasonic motors in actuator applications.[17]

While NBT forms a solid solution with ST, the 6s orbital in the Bi^{3+} position is replaced by the non-ferroelectric Sr^{2+} ion, weakening the lone pair activity. Thus, phase transformations vary significantly depending on the Sr^{2+} amount.[19] In the (1-x)NBT-x$SrTiO_3$ (denoted as NBT-ST) system near the morphotropic phase boundary (MPB) of $x = 0.25$, there are high P_{max} and low P_r values in the antiferroelectric-like double hysteresis curve. Thus, they are widely investigated for lead-free energy storage materials and for actuator applications.[20,21] Moreover, the properties of NBT systems in many studies can be regulated by using different preparation methods such as (1) addition of liquid phase sintering aid, (2) donor or acceptor doping to the A/B site in ABO_3 perovskite structure, (3) hot pressing (HP), (4) spark plasma sintering, and (5) templated grain growth (TGG) for texture formation.[22–28] Among these methods, texture formation based on nucleation and growth of textured grains on an oriented anisometric template particle is one of the most prevalent methods for modifying the piezoelectric properties and strain response. The basis of TGG is the orientation of template particles with a needle or plate-like morphology by shear force in the tape casting direction by a doctor blade.[28] BT, NN, ST, and NBT plate-like template particles have been used to develop the texture orientation of NBT-based systems.[26,28–30] However, the crystal structure compatibility, the template particle ratio, and the aspect ratio between the matrix and the template particle used in the texture formation also significantly affect the degree of orientation and the direct electrical and strain response.[28] 0.72NBT-0.28ST system was produced with the TGG method by Bai et al.[29] using 10% wt ST anisometric template particles, and the strain level was measured as 0.39% at 70 kV/cm, and the converse piezoelectric coefficient (d^*_{33}) as 557 pm/V.

The energy storage performance of pure and doped solid solutions of the NBT-0.25ST ceramics in bulk form has been investigated.[21,31,32] However, there are no further studies on the contribution of texturing to the strain behavior of the NBT-0.25ST. In this study, the effect of texturing on the electrical properties of NBT-0.25ST with NBT template particles on the electrical properties was investigated in detail for the first time in the literature.

2 | MATERIALS AND METHODS

The $0.75(Na_{0.5}Bi_{0.5})TiO_3$-$0.25SrTiO_3$ (NBT-0.25ST) powders were synthesized via a conventional solid-state reaction technique. The starting raw powders were chosen as Bi_2O_3 (Alfa Aesar, 99%), Na_2CO_3 (Sigma Aldrich), TiO_2 (Degussa, P25), and $SrCO_3$ (Sigma Aldrich ≥98%). Powders were ball-milled for 24 h in using zirconia balls as milling media and ethanol as milling medium and dried at 80°C. Then powders were calcined at 950°C for 4 h and then the ball-milling process was repeated for 24 h to break up the agglomerates.

In this study, texturing was provided in a NBT-0.25ST matrix system using 10 mol % NBT template particles. The details of the synthesis of <001> oriented plate-like NBT templates using a combination of molten salt synthesis and topochemical microcrystal conversation methods were given in previous works.[26,33] Both random and textured NBT-0.25ST slurries were prepared by using an organic binder solution and methyl ethyl ketone/ethanol mixture as a solvent, and then slurries were ball-milled for 24 h. NBT template particles were added and the slurry was mixed on a magnetic stirrer. The slurries were tape casted using a doctor blade at 10 cm/s casting rate. Random and textured NBT-0.25ST green tapes were stacked and laminated in a 15 mm diameter disk at 80 MPa. After removing the organic binder from the green compact by heating at 600°C with a 2°C/min heating rate, all ceramics were sintered at 1230–1260°C for 8 h in an air atmosphere in a double crucible arrangement to prevent Bi and alkali constituents volatilization. In this study, random and textured samples were named Random-1260 and Textured-1260, respectively. The schematic representation of textured NBT-0.25ST ceramics is given in Figure 1.

The <001> orientation degree of textured ceramics was calculated from the XRD pattern by Lotgering's method from Equations (1) and (2)[34]:

$$f_{(00l)} = \frac{P_T - P_R}{1 - P_R}, \quad (1)$$

$$P_{T,R} = \frac{[I_{(001)} + I_{(002)}]}{\sum I_{(hkl)}}, \quad (2)$$

where P_T and P_R are defined as the ratio of the intensities of all *(00l)* peaks to the total intensities of all XRD peaks for textured and randomly oriented ceramics.

The crystalline phases were detected using an X-ray diffractometer (XRD, Bruker D8 Advance, Bruker

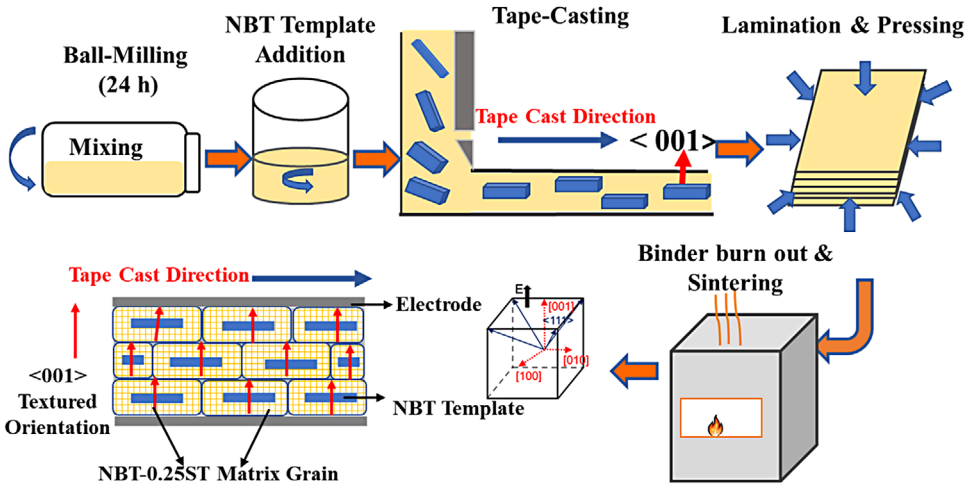

FIGURE 1 The schematic illustration of experimental stages of textured NBT-0.25ST ceramics.

AXS GmbH) with CuK$_\alpha$ radiation, $2\theta = 20°\sim70°$. The microstructural properties and elemental mapping analysis were investigated with a scanning electron microscope (SEM, Philips XL30 FEI Co.) with energy-dispersive X-ray spectrometry (EDS) on the fractured and polished surfaces of samples which were thermally etched at a temperature of 50°C below sintering temperature. The density of sintered ceramics was measured by the Archimedes' method. The ceramic pellets were polished and the silver paste electrode was screen-printed on both sides of the samples. Silver (Ag) electrode was fired at 600°C for 30 min for characterization of electrical properties. The temperature-dependence of dielectric constant (K) and loss tangent (tan δ) were taken using an inductance–capacitance–resistance (LCR) meter (Hioki 3532–50) at various frequencies (1–100 kHz) in between 25–500°C. The field-induced polarization and strain behavior of the ceramics were measured under 40 kV/cm electric field using a Precision LC ferroelectric tester (Radiant Technologies, Inc.) and MTI 2000 photonics sensor (MTI Instrument Inc.), respectively.

3 | RESULTS AND DISCUSSION

3.1 | Structural properties

The comparison of XRD patterns of random and textured NBT-0.25ST ceramics is represented in Figure 2A. As shown in Figure 2A, all ceramics were crystallized in a perovskite structure without any secondary phase. When compared, the (100) and (200) peaks of textured ceramics become stronger with increasing texture formation, while the other *(hkl)* peaks drastically decreased. Although the Lotgering factor was $f = 0.72$ in NBT-0.25ST textured ceramics sintered at 1230°C for 8 h, it reached

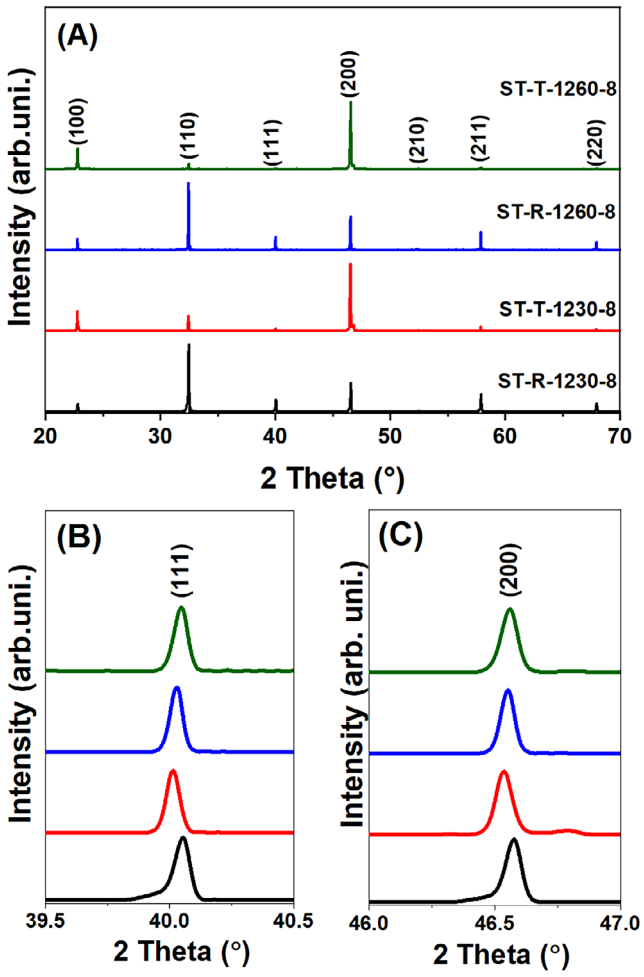

FIGURE 2 Normalized XRD patterns of random and textured NBT-0.25ST ceramics (A) full profile 2θ between 20° and 70° and (B) detailed profile of (111) peak between 39.5°−40.5° and (C) detailed profile of (200) peak between 46°−47°.

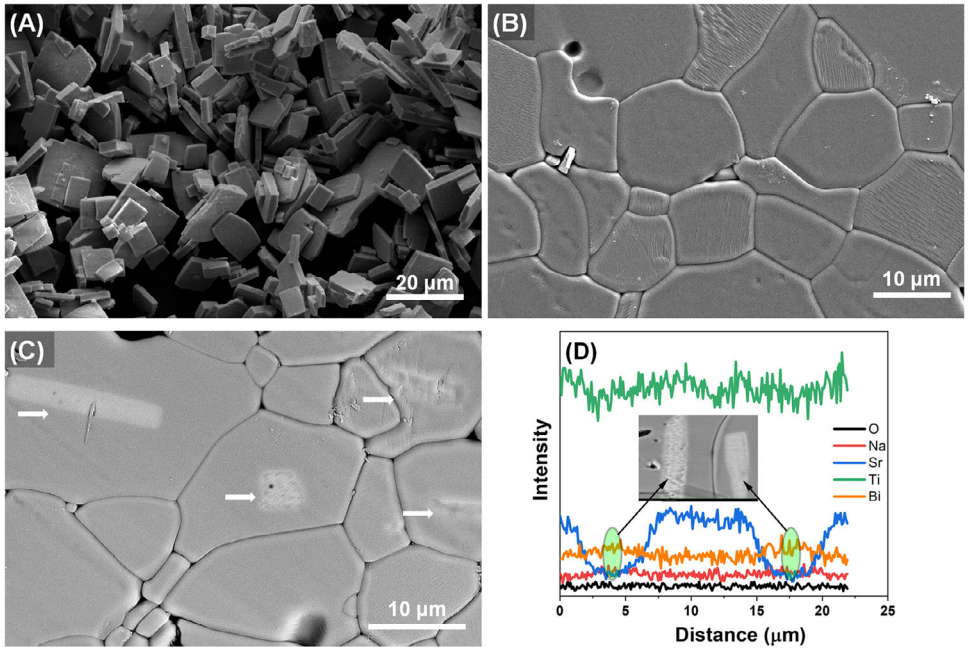

FIGURE 3 SEM micrographs of (A) plate-like NBT template, (B) polished surface, (C) cross-section surface of textured NBT-0.25ST ceramics, and (D) line EDS scan across two NBT templates in NBT-0.25ST matrix region.

0.88 in NBT-0.25ST textured ceramics sintered at 1260°C for 8 h. Obviously, it appears that increasing sintering temperature directly affects the texture formation kinetics.[35] XRD analysis results of (111) and (200) planes are given in Figure 2B,C. Replacement of Sr^{2+} ion to sodium or bismuth sites distorts the perovskite cell by changing interplanar spacing of planes due to slight ionic radius differences which also creates strain in the $(Na_{0.5}Bi_{0.5})TiO_3$ lattice.[36] Although they have similar crystal symmetries, the difference between the lattice parameters of the NBT templates and the NBT-ST matrix may cause distortion, and therefore lattice strain is generated with the growth of NBT-ST grain on the NBT templates during the TGG process. Thus, peak shifting occurs. Since no evidence of peak separations belonging to tetragonal or rhombohedral symmetries is observed, it is understood that both random and textured samples have a pseudocubic structure.[37]

The SEM micrograph of NBT template particles with plate-like morphology that were used in the study is given in Figure 3A. The aspect ratio (edge length to thickness) of NBT template particles is ~8 μm which is deemed suitable for texture formation with TGG. In Figure 3B, the surface microstructure of the polished and thermally etched textured NBT-0.25ST ceramics sintered at 1260°C for 8 h is given. Figure 3C, which is a backscattered electron image, also exhibits the microstructure of polished cross-section of textured NBT-0.25ST ceramics. The template grain growth can be explained by Oswald ripening due to the energy difference between template particles as the nucleation seed and the matrix grains.[38] To understand the interaction between NBT-0.25ST matrix/NBT template/matrix interface in more detail, two NBT templates and NBT-0.25ST textured grains were chosen and scanned. EDS line analysis is shown in Figure 3D. It is clear from the intensity variation of scan lines at the template-grain interface that Sr^{2+} ions are completely confined in the NBT-0.25ST matrix region. This indicates that the NBT template is stable without dissolving in the matrix.[36]

Figure 4 shows the SEM-EDS elemental distribution mapping analysis taken from the polished and thermally etched surfaces of textured NBT-0.25ST ceramics. This analysis focused on the interaction between textured grain and NBT template particles. These results show that the NBT template remains stable in the matrix and when the Sr, Na, Ti, and Bi distributions are examined; it indicates that there is no Sr template diffusion from the matrix in the template, and the template stays stable at high temperatures.

3.2 | Electrical properties

The comparison of temperature-dependent variation at dielectric constant (K) and loss tangent (tan δ) at various frequencies (1–100 kHz) for both random and textured NBT-0.25ST ceramics are presented in Figure 5A,B, respectively. Most NBT-based ceramic compositions have dielectric anomalies depending on temperature. Two anomalies were observed for both samples as expected: the first broadening peak belongs to anomaly at lower

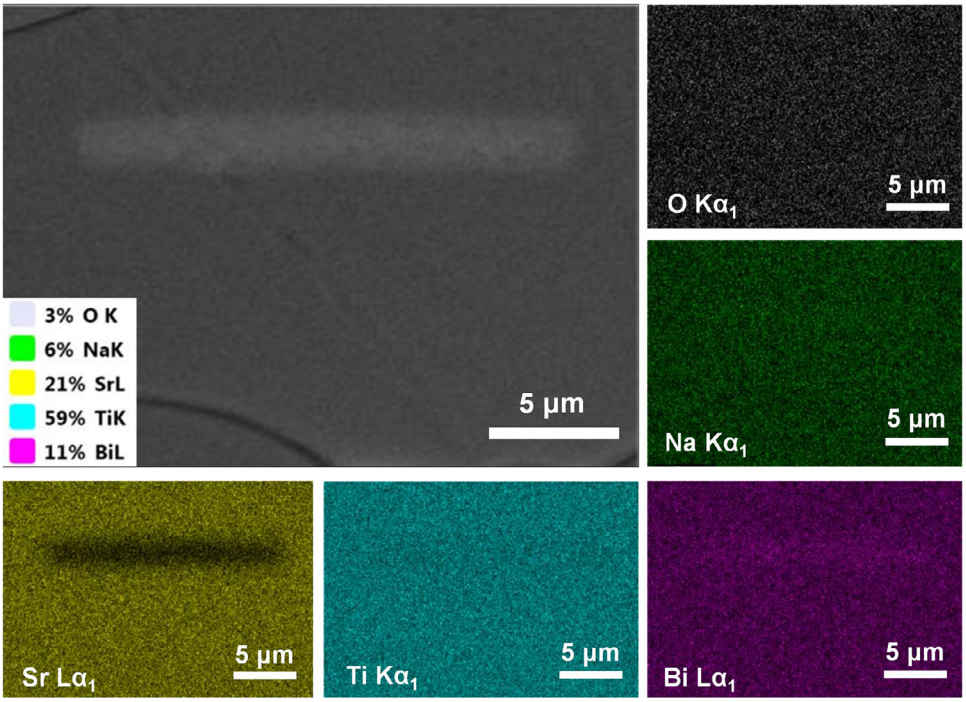

FIGURE 4 SEM micrograph and EDS mapping of textured NBT-0.25ST ceramics.

temperature ($T_{F\text{-}R}$)[37] and the second one is the maximum dielectric constant temperature (T_m). The first peak indicates strong frequency dependence and thermally driven transformation of a mixture of rhombohedral and tetragonal polar nanoregions (PNRs). The second peak is due to the phase transformation sequence of PNRs observed in relaxor ferroelectrics at high temperatures.[39] $T_{F\text{-}R}$ can be associated with the thermal activation of PNRs resulting from the relaxation behavior of dielectric materials in a limited temperature range below the Burns temperature (T_B).[41,42] NBT templates were used for texturing in this study, and they do not act as additional material such as ST or BT templates as used in another study in the literature. Thus, $T_{F\text{-}R}$ and T_m temperatures of random and textured NBT-0.25ST ceramics were not shifted.[41]

While the value of maximum dielectric constant (K_{max}) at 100 kHz of random ceramic was measured as 4041 at T_m, K_{max} of textured ceramic was found to be as 4182 as given in Table 1 with the other electrical measurement results. As given in Table 1, dielectric properties did not change drastically by texturing the ceramic with NBT templates.

Figure 6A shows the comparison of field-induced hysteresis loops for both random and textured ceramics measured at room temperature under 40 kV/cm and at 1 Hz. As shown in Figure 6A, all ceramics exhibit double-like hysteresis behavior with a low remnant polarization (P_r) value, and it was observed that this hysteresis pinches from the midsection. It is known that the ST ratio has a

TABLE 1 The comparison of electrical and electromechanical properties of random and textured NBT-0.25ST ceramics.

Properties	NBT-0.25ST-R (this study)	NBT-0.25ST-T (this study)	NBT-0.28ST-T[29]
Template	–	NBT (10 mol%)	ST (10 wt.%)
Lotgering factor	–	0.88	0.82
Relative density	93%	96%	
K (100 kHz @RT)	1517	1527	–
K_{max} (100 kHz)	4041	4182	–
tan δ (100 kHz @RT)	0.06	0.06	–
T_m (°C)	292	301	–
Unipolar strain (%)	0.09	0.59	0.39
Max. d^*_{33} (pm/V) (@10 kV/cm)	411	1021	–
Max. d^*_{33} (pm/V) (@40 kV/cm)	222	1488	557
P_{max} (μC/cm^2) (@40 kV/cm)	23.8	30.0	–
P_r (μC/cm^2) (@40 kV/cm)	2.82	6.60	–
E_c (kV/cm)	4.60	9.86	–
H (%) (@40 kV/cm)	35	47	–
Q_{33} (m^4/C^2)	0.025	0.059	–

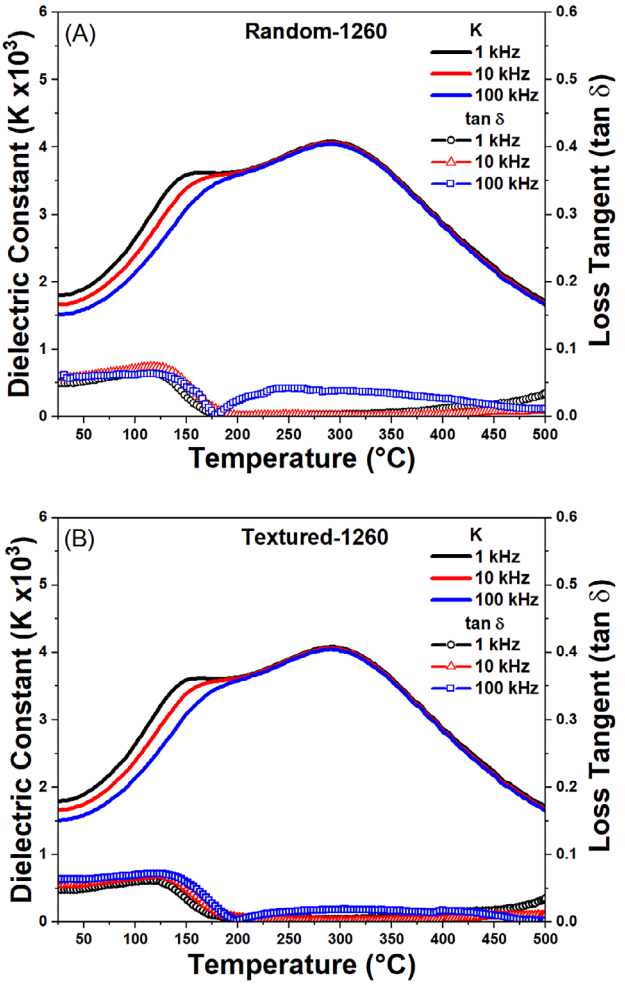

FIGURE 5 Temperature dependence of dielectric constant (K) and dielectric loss (tan δ) as a function of frequency for (A) random and (B) textured NBT-0.25T ceramics.

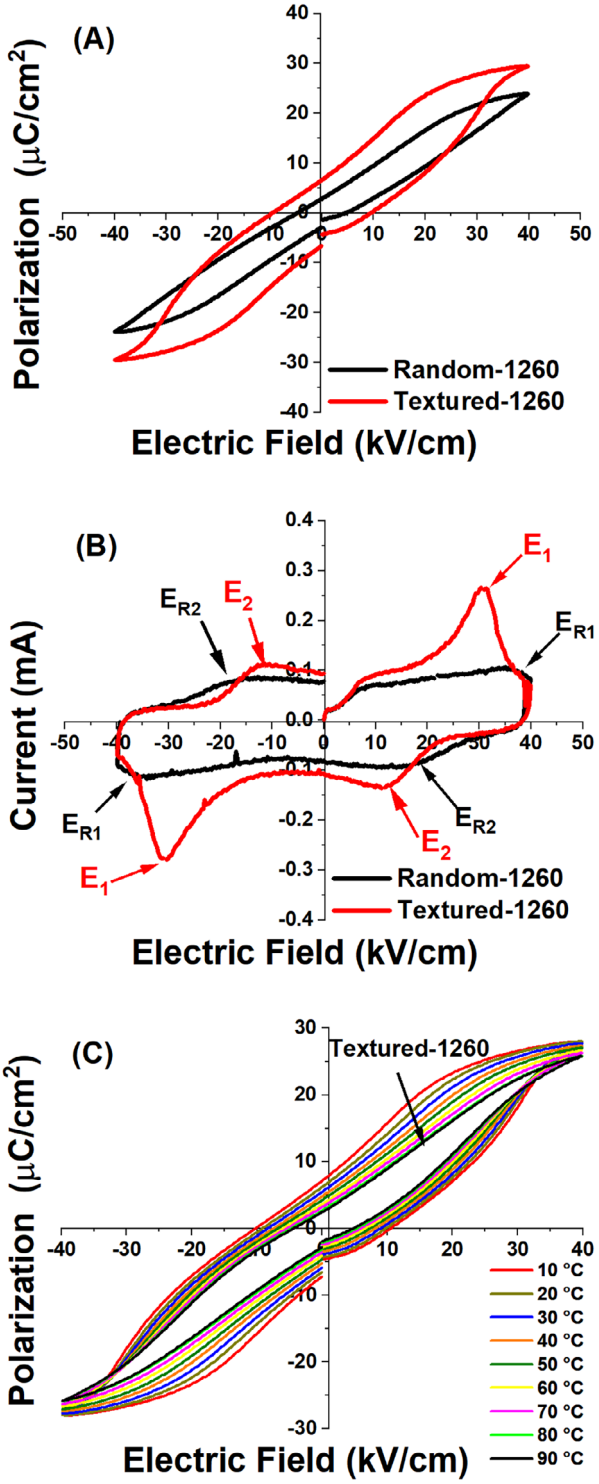

FIGURE 6 The comparison of (A) P–E hysteresis, (B) I–V loops of random and textured NBT-0.25ST, and (C) temperature-dependent hysteresis loops of textured ceramic.

very critical role in the hysteresis behavior of (1-x)NBT-xST systems. NBT-0.25ST has a normal ferroelectric hysteresis loop at an ST ratio of $x = 0.10$, while double hysteresis behavior was observed with an increasing ST ratio.[21] The P_r and maximum polarization (P_{max}) values increased with <001> textured orientation. P_r and P_{max} values of random and textured ceramics increased from 2.8 and 23.8 μC/cm^2 to 6.6 and 30.0 μC/cm^2, respectively. It was observed that the coercive field (E_c) value of textured NBT-0.25ST ceramics is higher than random samples. Figure 6B shows the current density vs. electric field curves of ceramics at 40 kV/cm electric field. Two sharp peaks (E_1) indicate the domain switching that is observed in normal ferroelectrics.

Nevertheless, in relaxor-based materials, additional two peaks, denoted as E_2, are observed near E_1 peaks, and in this case, two-step polarization can be associated with domain switching.[43,44] As the electric field was increased, a forward switching from nonpolar relaxor to normal ferroelectric phase occurred at E_1 and a backward switching occurred at E_2. In Figure 6B, E_1 and E_2 are indicated for textured ceramics, while E_{R1} and E_{R2} are expressed for randomly oriented ceramics.

Temperature-dependent P–E loops of textured NBT-0.25ST ceramics in the range from 90°C to 10°C in the

cooling regime are given in Figure 6C. There was not any change in the characteristic of the hysteresis loops of textured ceramic by increasing temperature. P–E loops became slimmer which means less loss and the values of E_c, P_r, and P_{max} decreased by increasing temperature. Increasing temperature activates the locked domain walls and then easy domain motion occurs. The fatigue behavior of ceramics is very important for device applications. Defect formation with dopant contribution and texture orientation are effective solutions for regulating the fatigue behavior of ceramics.[45,46] Leng et al.[46] determined that the textured 2 mol% MnO_2 and 0.25 wt% CuO-doped 0.24PIN−0.42PMN−0.34PT system had a higher fatigue resistance behavior compared with the counterpart doped random sample.

After dielectric and ferroelectric measurements, the room temperature field-induced strain behavior of random and textured NBT-0.25ST ceramics were measured using a triangular waveform at 1 Hz and the results were given in Figure 7A. Both ceramics exhibited a tulip-shaped curve with zero negative strain (s_{neg}) that is characteristic of the field-induced phase change materials which results in decreased ferroelectric character while evaluation of ergodic state.[47] The most remarkable result of the current study is that while the bipolar maximum strain (s_{max}) value is measured as 0.13% for random ceramic, the s_{max} value is found to be as 0.51% for textured one. Both samples exhibited relaxor behavior as seen in Figure 5. Relaxor ferroelectrics have PNRs that exhibit local polarization regions. These PNRs are disordered and interact with each other. When the external electric field was applied, PNRs contributed to the overall strain and electromechanical properties of the relaxor ferroelectric material. Besides this, as seen in Figure 6, texturing the NBT-0.25ST relaxor ferroelectric material involves aligning the crystallographic axes in a preferred direction. Texturing enhances the strain response along the preferred orientation for relaxor NBT-0.25ST.

In NBT-based piezoelectrics, the 180° domains normally can lead to high-strain behavior which does not switch normally with the electric field.[32] The ultra-high strain occurring in NBT-based systems can be attributed to its co-existence with non-ergodic and ergodic phases.[44]

Electrostriction is typically an electromechanical effect that could occur in all dielectric materials and is expressed as following (Equation 3):

$$s = Q_{33}P^2, \quad (3)$$

where s, Q_{33}, and P are strain, electrostrictive coefficients, and polarization, respectively.[18,47,48] Figure 7B also gives s-P^2 plots with relating square of polarization and unipolar strain loops of both NBT-0.25ST ceramics. The Q_{33}

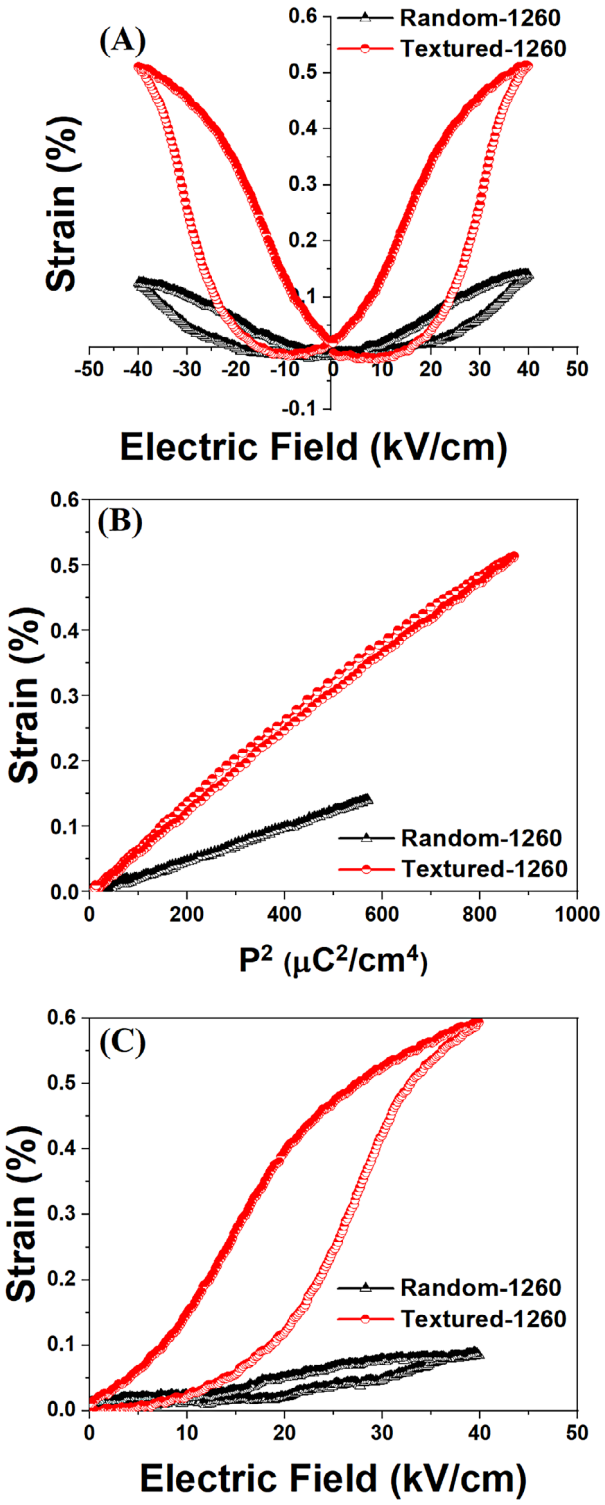

FIGURE 7 The comparison of (A) bipolar strain as a function of an electric field, (B) strain as a function of P^2, and (C) unipolar strain for of random and textured NBT-0.25ST ceramics.

values of random and textured NBT-0.25ST ceramics are calculated as 0.025 and 0.059 m^4/C^2, respectively. The unipolar strains also display an important role in the real performance of the practical actuator applications.[17] The unipolar strain curves of both random and textured

ceramics are given in Figure 7C. The maximum unipolar strain values of random and textured NBT-0.25ST systems are found to be as ~0.09% and ~0.59%, respectively. These results are comparable with the bipolar strain levels.

One of the mechanisms for the large strain of the textured ceramic may be a combination of a volume change during a field-induced phase transition.[49] The electric field-induced structural phase transformation was the microstructural origins for the large strain. Another mechanism for the large strain response of the textured NBT-0.25ST ceramic can be the increasing grain orientation.[50] As a result, the large macroscopic strain can arise from the combination of the electric field-induced phase transition and grain orientation.[51] The high field converse piezoelectric charge coefficients (d^*_{33})values of random and textured NBT-0.25ST ceramics at 40 kV/cm electric field are found to be as 222 and 1488 pm/V, respectively. The hysteresis H% ($\Delta s/s_{max}$) values of all ceramics were calculated from the unipolar *s-E* hysteresis loops and given in Table 1.

Figure of merit (FOM) depends on the piezoelectric charge and voltage coefficients, that is, $d^*_{33}xg_{33}$, where the piezoelectric voltage coefficient, g_{33}, is in turn directly proportional to d^*_{33} and inversely proportional to the dielectric constant K. While FOM of random sample was calculated to be ~3670 × 10^{-15} m^2/N, FOM of the textured one was calculated as 163 680 × 10^{-15} m^2/N under high field. It is obvious result that FOM of the random sample was increased ~45-fold with texture. The FOM under low electric fields of textured NBT-0.25 ST was found to increase almost sixfold compared with the random sample.

4 | CONCLUSION

In summary, <001> oriented NBT-0.25ST textured ceramics were fabricated with 88% texture orientation using the TGG method. The textured NBT-0.25ST ceramic exhibits 45 times larger strain values compared with the random one, and this behavior can be attributed to both electric field-induced phase transition and grain orientation. These mechanisms contribute to the material's ability to undergo significant strain under the influence of an electric field. This implies that the alignment or orientation of the individual grains in the material plays a role in generating a significant macroscopic strain when subjected to an electric field. In summary, this improvement in the FOM can be attributed to the previously mentioned mechanisms, such as the electric field-induced phase transition and grain orientation, which enhance the material's response to electric fields and, consequently, its performance.

ACKNOWLEDGEMENTS

The authors acknowledge the financial support of Bursa Technical University, Scientific Research Projects Coordinatorship for research funding with grant number 211N046.

Open access funding is enabled and organized by TUBITAK ULAKBIM.

CONFLICT OF INTEREST STATEMENT

The authors declare no conflict of interest.

ORCID

Ayse Berksoy-Yavuz https://orcid.org/0000-0002-6462-343X

Mustafa Yunus Kaya https://orcid.org/0000-0002-4518-3184

Ezgi Yalcin https://orcid.org/0000-0001-7465-0047

Namik Kemal Gozuacik https://orcid.org/0000-0003-3021-0933

Ebru Mensur https://orcid.org/0000-0001-7045-9771

REFERENCES

1. Tressler JF, Alkoy S, Newnham RE. Piezoelectric sensors and sensor materials. J Electroceram. 1998, 2:257–72.
2. Sugawara Y, Onitsuka K, Yoshikawa S, Xu Q, Newnham RE, Uchino K. Metal–ceramic composite actuators. J Am Ceram Soc. 1992, 75(4):996-98.
3. Sarjeant WJ. Capacitors. IEEE Trans Dielectr Electr Insul. 1990;25(5):861-922.
4. Alkoy S, Dogan A, Hladky A-C, Langlet P, Cochran JE, Newnham NE, et al. Miniature piezoelectric hollow sphere transducers (BBs). IEEE Trans Ultrason Ferroelectr Freq Control. 1997, 44(5):1067-76.
5. Hagood NW, Mcfarland AJ. Modeling of a piezoelectric rotary ultrasonic motor. IEEE Trans Ultrason Ferroelectr Freq Control. 1995, 42(2):210-24.
6. Yan Y, Wang YU, Priya S. Electromechanical behavior of [001]-textured $Pb(Mg_{1/3}Nb_{2/3})$ O_3-$PbTiO_3$ ceramics. Appl Phys Lett. 2012, 100(19):192905
7. Berksoy-Yavuz A, Mensur-Alkoy E, Erdem E, Alkoy S. Electrical properties, EPR analyses and defect chemistry of Mn-doped 0.675PMN-0.325PT piezoceramics. Ceram Int. 2020, 46(18):28980-86
8. Kaya MY, Mensur-Alkoy E, Gurbuz A, Oner M, Alkoy S. Influence of compositional variation on the electrical properties of $[Pb(Zn_{1/3}Nb_{2/3})O_3]$–$[Pb(Zr,Ti)_{O3}]$ ceramics and their transducer application. IEEE Trans Ultrason Ferroelectr Freq Control. 2018, 65(7):1268–77.
9. Berksoy-Yavuz A, Mensur-Alkoy E, Gozutok E, Dursun S, Yilmaz H, Alkoy S. Structural and electrical properties of <001>textured 0.26PIN–0.40PMN–0.34PT ternary system. J Mater Sci Mater. 2019, 30:18548-56.
10. EU-Directive 2002/95/EC. Restriction of the use of certain hazardous substances in electrical and electronic equipment (RoHS), Official Journal of the European Union (OJEU). 2003, 46(L37):19.

11. Rödel J, Jo W, Seifert KTP, Anton E-M, Granzow T, Damjanovic D. Perspective on the development of lead-free piezoceramics. J Am Ceram Soc. 2009, 92(6):1153-77.
12. Smolenskii GA, Agranovskaya AI, Popov SN, et al. New ferroelectrics of complex composition. Sov Phys Tech Phys. 1958, 28:2152.
13. Takenaka T, Kei-Ichi Maruyama K-IM, Koichiro Sakata KS. $(Bi_{1/2}Na_{1/2})TiO_3$-$BaTiO_3$ system for lead-free piezoelectric ceramics. Jpn J Appl Phys. 1991, 30(9S):2236.
14. Gomah-Pettry J. Sodium-bismuth titanate based lead-free ferroelectric materials. J Eur Ceram. 2004, 24(6):1165-69.
15. Sakata K, Masuda Y. Ferroelectric and antiferroelectric properties of $(Na_{0.5}Bi_{0.5})TiO_3$-$SrTiO_3$ solid solution ceramics. Ferroelectrics. 1974, 7(1):347-49.
16. Takenaka T, Okuda T, Takegahara K. Lead-free piezoelectric ceramics based on $(Bi_{1/2}Na_{1/2})TiO_3$-$NaNbO_3$. Ferroelectrics. 1997, 196(1):175-78.
17. Zhu Y, Zhang Y, Xie B, Fan P, Marwat MA, Ma W, et al Large electric field-induced strain in $AgNbO_3$-modified $0.76Bi_{0.5}Na_{0.5}TiO_3$-$0.24SrTiO_3$ lead-free piezoceramics. Ceram Int. 2018, 44(7):7851-57.
18. Dinh TH, Han H-S, Lee J-S. Large strain response under low field in $SrTiO_3$ modified $Bi_{1/2}Na_{1/2}TiO_3$-$LaFeO_3$ piezoceramics. Mater Lett. 2020, 258:126793.
19. Liu X, Xue S, Wang F, Zhai J, Shen B. Grain size dependent physical properties in lead-free multifunctional piezoceramics: a case study of NBT-xST system. Acta Mater. 2019, 164:12-24.
20. Yang Z, Gao F, Du H, Jin Li, Yan L, Hu Q, et al. Grain size engineered lead-free ceramics with both large energy storage density and ultrahigh mechanical properties. Nano Energy. 2019, 58:768-77.
21. Cao WP, Li WL, Dai XF, Zhang TD, Sheng J, Hou YF, et al. Large electrocaloric response and high energy-storage properties over a broad temperature range in lead-free NBT-ST ceramics. J Eur Ceram. 2016, 36(3):593-600.
22. Eglite L, Antonova M, Birks E, Knite M, Livinsh M. Grain growth in $Na_{0.5}Bi_{0.5}TiO_3$-based solid solutions. Integr Ferroelectr. 2019, 196(1):112-19.
23. Li M, Li L, Zang J, Sinclair DC. Donor-doping and reduced leakage current in Nb-doped $Na_{0.5}Bi_{0.5}TiO_3$. Appl Phys Lett. 2015, 106(10):102904.
24. Shih DPC, Aguadero A, Skinner SJ. A-site acceptor-doping strategy to enhance oxygen transport in sodium–bismuth–titanate perovskite. J Am Ceram Soc. 2023, 106(1):100-108.
25. Mudinepalli VR, Leng F, Reddy MP, Lin WC, Murty BS. Structural, dielectric and ferroelectric properties of lead-free $Na_{0.5}Bi_{0.5}TiO_3$ ceramics prepared by spark plasma sintering technique. Ind J Phys. 2016, 90:131-38.
26. Berksoy-Yavuz A, Kaya MY, Avcı T, Cakırbas G, Menşur E. Fabrication of 0.94 NBT–0.06BT textured ceramics using plate-like NBT templates and their electrical properties. J Mater Sci Mater. 2022, 33:2336–49.
27. Zhang H, Wei T, Zhang Qi, Ma W, Fan P, Salamon D, et al. A review on the development of lead-free ferroelectric energy-storage ceramics and multilayer capacitors. J Mater Chem C. 2020, 8(47):16648-67.
28. Messing GL, Trolier-Mckinstry S, Sabolsky EM, Duran C, Kwon S, Brahmaroutu B, et al. Templated grain growth of textured piezoelectric ceramics. Crit Rev Solid State Mater Sci. 2004, 29(2):45-96.
29. Bai W, Hao J, Fu F, Li W, Shen B, Zhai J. Structure and strain behavior of <001> textured BNT-based ceramics by template grain growth. Mater Lett. 2013, 97;137-40.
30. Fan P, Liu K, Ma W, Tan H, Zhang Q, Zhang L, et al. Progress and perspective of high strain NBT-based lead-free piezoceramics and multilayer actuators. J Mater. 2021, 7(3):508-44.
31. Cao W, Lin R, Chen P, Li F, Ge B, Song D., et.al. Phase and band structure engineering via linear additive in NBT-ST for excellent energy storage performance with superior thermal stability. ACS Appl Mater Interfaces. 2022, 14:54051.
32. Li T, Chen P, Li F, Wang C. Energy storage performance of $Na_{0.5}Bi0_{.5}TiO_3$-$SrTiO_3$ lead-free relaxors modified by $AgNb_{0.85}Ta_{0.15}O_3$. J Chem Eng. 2021, 406:127151.
33. Dursun S, Mensur-Alkoy E, Sabuncu A, Berksoy-Yavuz A, Gülgün MA, Alkoy S. Growth of NBT template particles through topochemical microcrystal conversion and their structural characterization. J Am Ceram Soc. 2017, 100(3):937-44.
34. Lotgering FK. Topotactical reactions with ferrimagnetic oxides having hexagonal crystal structures-I. J Inorg Nucl Chem. 1959, 9(2):113-23.
35. Sabolsky EM, Messing GL, Trolier-Mckinstry S. Kinetics of templated grain growth of $0.65Pb(Mg_{1/3}Nb_{2/3}O_3{\cdot}0.3PbTiO_3)$. J Am Ceram Soc. 2001, 84(11):2507-13.
36. Cui C, Pu Y, Gao Z, Wan J, Guo Y, Hui C., et.al. Structure, dielectric and relaxor properties in lead-free ST-NBT ceramics for high energy storage applications. J Alloys Compd. 2017, 711:319-26.
37. Acosta M, Jo W, Rödel J. Temperature and frequency dependent properties of the $0.75Bi_{1/2}Na_{1/2}TiO_3$–$0.25SrTiO_3$ lead-free incipient piezoceramic. J Am Ceram Soc. 2014, 97(6):1937–43.
38. Maurya D, Zhou Y, Wang Y, Yan Y, Li J, Viehland D, et al. Giant strain with ultra-low hysteresis and high temperature stability in grain oriented lead-free $K_{0.5}Bi_{0.5}TiO_3$-$BaTiO_3$-$Na_{0.5}Bi_{0.5}TiO_3$ piezoelectric materials. Sci Rep. 2015, 5(1):8595.
39. Akça E, Duran C, Kowalski B, Sehirlioglu A. Templated grain growth of $Bi(Zn_{0.5}Zr_{0.5})O_3$ modified $BiScO_3$−$PbTiO_3$ piezoelectric ceramics for high temperature applications. J Asian Ceram Soc. 2021, 9(3):874-81.
40. Chen M, Pu Y, Zhang L. Novel NBT-based relaxor ferroelectric ceramics with excellent discharge performance and high-temperature stability. J Mater Sci Mater. 2021, 32(18):23540-53.
41. Amorín H, Uršič H, Ramos P, Holc J, Moreno R, Chateigner D, et al. $Pb(Mg_{1/3}Nb_{2/3})O_3$-$PbTiO_3$ textured ceramics with high piezoelectric response by a novel templated grain growth approach. J Am Ceram Soc. 2014, 97(2):420–26.
42. Lou G, Yin Q, Duan A, Cao D, Yin X. Structure, dielectric properties and impedance analysis of lead-free $(1-x)Na_{0.5}Bi_{0.5}TiO_3$-$xSrTiO_3$ ceramics. J Mater Sci Mater. 2018, 29:6283-88.
43. Liu X, Zhai J, Shen Bo, Li F, Zhang Y, Li P, et al. Electric-field-temperature phase diagram and electromechanical properties in lead-free $(Na_{0.5}Bi_{0.5)}TiO_3$-based incipient piezoelectric ceramics. J Eur Ceram. 2017, 37(4):1437-47.
44. Gozuacik NK, Bayir MC, Mensur-Alkoy E, Alkoy S. Origin of the large field-induced strain and enhanced energy storage response of rare-earth-doped lead-free 0.854BNT–0.12BKT–0.026BT ceramics. IEEE Trans Ultrason Ferroelectr Freq Control. 2021, 68(7):2576-84.

45. Jia X, Zhang J, Wang L, Wang J, Du H, Yao Y, et al. Role of oxygen-vacancy in piezoelectric properties and fatigue behavior of $(Bi_{0.5}Na_{0.5})_{0.93}Ba_{0.07}Ti_{1+x}O_3$ ceramics. J Am Ceram Soc. 2019, 102:5203–12.
46. Leng H, Yan Y, Fanton M, Priya S. Polarization fatigue mechanism of high-power textured piezoelectric ceramics. ACS Appl Electron Mater. 2022, 4 (3):1047–56.
47. Jo W, Dittmer R, Acosta M, Zang J, Groh C, Sapper E, et al. Giant electric-field-induced strains in lead-free ceramics for actuator applications–status and perspective. J Electroceram. 2012, 29:71-93.
48. Alkoy EM, Berksoy A, Tekdas AS. Electric field-induced strain behavior in lithium-and copper-added potassium sodium niobate piezoceramics and 1–3 piezocomposites. IEEE Trans Ultrason Ferroelectr Freq Control. 2011, 58(9):1804-10.
49. Fu F, Zhai J, Xu Z, Bai W, Yao Xi. Electric properties of high strain textured $Na_{0.5}Bi0_{.5}TiO_3$–$BaTiO_3$–$K_{0.5}Na_{0.5}NbO_3$ thick films. Solid State Sci. 2011, 13(5):934-37.
50. Jiang C, Zhou X, Zhou K, Chen C, Luo H, Yuan Xi, et al. Grain oriented $Na_{0.5}Bi_{0.5}TiO_3$-$BaTiO_3$ ceramics with giant strain response derived from single-crystalline $Na_{0.5}Bi_{0.5}TiO_3$-$BaTiO_3$ templates. J Eur Ceram. 2016, 36(6):1377-83.
51. Chen C, Zhao X, Wang Y, Zhang H, Deng H, Li X, et al. Giant strain and electric-field-induced phase transition in lead-free $(Na_{0.5}Bi_{0.5})TiO_3$-$BaTiO_3$-$(K_{0.5}Na_{0.5})NbO_3$ single crystal. Appl Phys Lett. 2016, 108(2):022903.

How to cite this article: Berksoy-Yavuz A, Kaya MY, Yalcin E, Gozuacik NK, Mensur E. Effect of texture on ultra-high strain behavior in eco-friendly NBT-0.25ST ceramics using NBT template. J Am Ceram Soc. 2024;107:5502–11.
https://doi.org/10.1111/jace.19834